TECHNICAL REPORT ARBRL-TR-02246

WIND TUNNEL MEASUREMENTS OF SABOT DISCARD AERODYNAMICS

Edward M. Schmidt

July 1980

US ARMY ARMAMENT RESEARCH AND DEVELOPMENT COMMAND
BALLISTIC RESEARCH LABORATORY
ABERDEEN PROVING GROUND, MARYLAND

Destroy this report when it is no longer needed.
Do not return it to the originator.

Secondary distribution of this report by originating or sponsoring activity is prohibited.

Additional copies of this report may be obtained from the National Technical Information Service, U.S. Department of Commerce, Springfield, Virginia 22151.

The findings in this report are not to be construed as an official Department of the Army position, unless so designated by other authorized documents.

The use of trade names or manufacturers' names in this report does not constitute indorsement of any commercial product.

UNCLASSIFIED

SECURITY CLASSIFICATION OF THIS PAGE *(When Data Entered)*

REPORT DOCUMENTATION PAGE

READ INSTRUCTIONS BEFORE COMPLETING FORM

1. REPORT NUMBER: TECHNICAL REPORT ARBRL-TR-02246
2. GOVT ACCESSION NO.:
3. RECIPIENT'S CATALOG NUMBER:

4. TITLE *(and Subtitle)*: Wind Tunnel Measurements of Sabot Discard Aerodynamics

5. TYPE OF REPORT & PERIOD COVERED: Final

6. PERFORMING ORG. REPORT NUMBER:

7. AUTHOR(s): Edward M. Schmidt

8. CONTRACT OR GRANT NUMBER(s):

9. PERFORMING ORGANIZATION NAME AND ADDRESS:
US Army Ballistic Research Laboratory
(ATTN: DRDAR-BLL)
Aberdeen Proving Ground, MD 21005

10. PROGRAM ELEMENT, PROJECT, TASK AREA & WORK UNIT NUMBERS: 1L162618AH80

11. CONTROLLING OFFICE NAME AND ADDRESS:
US Army Armament Research & Development Command
US Army Ballistic Research Laboratory
(ATTN: DRDAR-BL)
Aberdeen Proving Ground, MD 21005

12. REPORT DATE: July 1980

13. NUMBER OF PAGES: 43

14. MONITORING AGENCY NAME & ADDRESS *(if different from Controlling Office)*:

15. SECURITY CLASS. *(of this report)*: Unclassified

15a. DECLASSIFICATION/DOWNGRADING SCHEDULE:

16. DISTRIBUTION STATEMENT *(of this Report)*

Approved for public release; distribution unlimited.

17. DISTRIBUTION STATEMENT *(of the abstract entered in Block 20, if different from Report)*

18. SUPPLEMENTARY NOTES

19. KEY WORDS *(Continue on reverse side if necessary and identify by block number)*

Sabot
Aerodynamics
Launch Dynamics
Kinetic Energy Projectiles

20. ABSTRACT *(Continue on reverse side if necessary and identify by block number)* (ner)

This report addresses the flow field around a fin stabilized, hypervelocity projectile during the sabot discard process. The mutual interference of the flows around the flight body and three sabot components is examined through wind tunnel tests conducted at a free stream Mach number of 4.5. Since it was not practical to attempt the actuation of all three sabot components, the flow field was simulated by using splitter plates to develop reflection surfaces along planes of symmetry. The data show the effects of multiple shock interactions, shock-boundary layer interactions, and the variation in aerodynamic loadings as

DD FORM 1 JAN 73 1473 EDITION OF 1 NOV 65 IS OBSOLETE

UNCLASSIFIED

SECURITY CLASSIFICATION OF THIS PAGE *(When Data Entered)*

the sabot discard proceeds.

TABLE OF CONTENTS

		Page
	LIST OF FIGURES	5
I.	INTRODUCTION	7
II.	BALLISTIC RANGE DATA	8
III.	MODEL DESIGN AND TEST PROCEDURE	9
IV.	TEST RESULTS	10
	A. Sabot Alone	10
	B. Symmetry Analysis	11
	C. Wave Form Analysis	12
	D. Sabot Discard Sequence	13
V.	SUMMARY AND CONCLUSIONS	15
	ACKNOWLEDGMENT	34
	REFERENCES	35
	DISTRIBUTION LIST	37

LIST OF FIGURES

Figure		Page
1.	Typical Saboted Projectile: 60mm Round.	16
2.	Schematic of Post-Launch Disturbances	16
3.	Sample X-ray Sequence of the Sabot Discard from 75mm Round Launched from Smoothbore Gun	17
4a.	Measured Variation in Sabot Angle of Attack During Discard	18
4b.	Measure Variation in Sabot Lateral Separation During Discard	18
5.	Separation Coordinates	19
6.	Photograph of Sabot and Projectile with Splitter Plates Installed	19
7.	Photograph of Three Sabot Components and Projectile .	20
8a.	Scaled Dimensions (d = 0.0508m, 2")	20
8b.	Scaled Dimensions (d = 0.0508m, 2")	21
8c.	Scaled Dimensions (d = 0.0508m, 2")	21
9.	Variation in Pressure Distribution Along Centerline of Sabot with Sabot Mounted Independently in Wind Tunnel	22
10.	Pressure Distributions Along Centerlines of Sabot and Projectile for Symmetry Check Cases, $\alpha = 0^{o}$, $\Delta X = 0$, $\Delta Y = 0.75$ d.	23
11a.	Pressure Contours on Projectile Surface for Symmetry Check Case	24
11b.	Pressure Contours on Sabot Surface for Symmetry Check Case	24
12a.	Projectile Centerline Pressure Distribution with Three Sabots Installed, One of which is being Traversed Forward.	25

LIST OF FIGURES (Continued)

Figure		Page
12b.	Sabot Pressure Distribution on Moving Sabot with Three Sabots Installed.	26
13.	Schematic of Shock Propagation Between Sabot and Projectile Viewed in Planes Perpendicular to the Projectile Axis of Symmetry at Sequential Axial Stations.	27
14a.	Pressure Distributions During Simulated Sabot Discard, $\alpha = 0^{o}$, $\Delta X = 0$, $\Delta Y = 0.64$ d.	29
14b.	Pressure Distributions During Simulated Sabot Discard, $\alpha = 4^{o}$, $\Delta X = 0$, $\Delta Y = 0.25$ d.	30
14c.	Pressure Distributions During Simulated Sabot Discard, $\alpha = 10^{o}$, $\Delta X = 0$, $\Delta Y = 0.25$ d	31
14d.	Pressure Distributions During Simulated Sabot Discard, $\alpha = 18^{o}$, $\Delta X = 0$, $\Delta Y = 0.5$ d	32
15.	Spark Shadowgraph of Flow over Nose of Saboted Projectile, $M_{\infty} = 1.4$.	33

I. INTRODUCTION

A sabot, Figure 1, is required to launch the current family of anti-armor, kinetic energy projectiles. Within the bore, the sabot provides gas sealing, structural support, and reduced sectional density. However, once free on the gun tube, the sabot must be discarded in order to permit unconstrained, low drag flight to the target. Typically, the sabot is divided into three or more components along axial planes. These components separate from the projectile under the action of elastic, inertial (gyroscopic), and aerodynamic loads. During this separation, a variety of interactions between the components and flight body may occur to perturb the desired trajectory, Figure 2.

It has been domonstrated[1-3] that aerodynamic interference can be a significant source of launch disturbance. The perturbation is strengthened by geometric asymmetry in the discard pattern and its associated flow field, and by extended periods of flight of the sabot segments in close proximity to the projectile. The details of this hypervelocity, three-dimensional interference flow field are not well understood.

Considerable information is available dealing with interference flows associated with stores separation from aircraft, generally flying at subsonic or low supersonic velocities[4]. Additionally, wing-body and engine/intake-airframe interference is widely documented[5]. At higher velocities, data is available describing the flow about advanced aerodynamic flight bodies[6] and flow field related to three dimensional

---

1. *H. Conn, "The Influence of Sabot Separation on the Yawing Motion of a Cone," Defense Research Establishment at Valcartier, Canada, June 1970, TN 1849/70.*

2. *W. Glauz, "Estimation of Forces on a Flechette Resulting from a Shock Wave," Midwest Research Institute, Kansas City, MO, May 1971, R3450-E.*

3. *E. Schmidt and D. Shear, "Aerodynamic Interference During Sabot Discard," AIAA JSR, Vol. 15, No. 3, May-June 1978, pp 162-167.*

4. *Anon, "Proceedings of the Fourth Aircraft/Stores Compatibility Symposium," Joint Technical Coordinating Group for Munitions Development, Air Force Armaments Laboratory, Eglin, FL, 12-14 October 1977.*

5. *W. Sears, Ed., "Aerodynamic Interference," AGARD Conference Proceedings No. 71, September 1970.*

6. *W. Sayano, C. Erickson, and J. Murphy, "Aerodynamic Interference Associated with Two Parallel Bodies in Close Proximity in Hypersonic Flow," AFFDL, Wright-Patterson AFB, OH, TR AFFDL-64-158, December 1964.*

inlets[7,8]. However, a source describing the flow field about multiple bodies executing a wide range of relative geometric configurations at hypersonic velocities was not found.

This report describes the results of an experimental program to investigate the aerodynamics of sabot discard. Instrumented firings from ballistic ranges were used to establish the geometries of interest. A wind tunnel model was fabricated to a representative sabot/projectile design. Tests were conducted at the NASA Langley Unitary Plan Facility to measure preasure distributions on both the projectile and sabot. Based on the wind tunnel data, design modifications are suggested to improve discard.

II. BALLISTIC RANGE DATA

A wide variety of kinetic energy round designs have been tested. Two are selected as representative of current trends: a 23mm diameter projectile launched from a slow twist 60mm tube, Figure 1, and a 21mm diameter projectile launched from a smoothbore, 75mm tube. Both rounds employ similar sabot designs. The front of the four segment sabot is chamfered to provide a positive pitching moment and lift force once exposed to an oncoming stream. The rear of the sabot is a conical ramp. The ramp is designed to compress around the projectile within the bore. This provides support against tensile failure under high acceleration loadings.

Sabot discard is measured using six orthogonal X-ray stations positioned along the first 10m of the trajectory[3]. A typical set of radiographs show the sabot components pitching away from and lifting off the flight body, Figure 3. The measured separation kinematics are compared for the two designs in Figure 4 where the coordinates are given in Figure 5. The 75mm sabot components are seen to move more rapidly away from the projectile than do the 60mm sabot components. This is due to the design of the deep lifting cup on the front of the 75mm sabot and due to its fabrication from magnesium compared with aluminum used in the 60mm sabot. Also shown on this figure are the ranges within which wind tunnel tests were conducted. These boundaries were established by geometric constraints within the test arrangement; however, this test region includes the geometries of interest for strong mutual interaction.

---

7. *D. Knight, "Improved Numerical Simulation of High Speed Inlets Using the Navier-Stokes Equations," AIAA Paper 80-0383, January 1980.*

8. *R. Buggeln, H. McDonald, J. Kreskovsky, and R. Levy, "Computation of Three-Dimensional Viscous Supersonic Flows in Inlets," AIAA Paper No. 80-0194, January 1980.*

III. MODEL DESIGN AND TEST PROCEDURE

Since it was not practical to attempt a test program incorporating multiple actuated sabot components, a system was required to simulate the flow field about the configuration of interest but using only one driven sabot segment. Splitter plates were selected as a feasible means of generating reflecting planes of symmetry. Splitter plates have been used to test the dynamics of half bodies[9] and to examine the flow field and mutual interference between two bodies[10]. The resulting data were shown to agree well with full body results. In the present tests, the splitter plate technique is extended to simulate a trilaterally symmetric flow.

The configuration selected for testing is a three segment sabot, Figure 6. The 120^{o} included angle sabot component is positioned along the plane of symmetry of the splitter plates and projectile center body. The splitter plates act as reflecting surfaces along planes of symmetry in the trilaterally symmetric flow field. In order to use this technique, only discard from smoothbore guns can be considered since any precessional, rolling, or yawing motion would destroy the symmetry of the flow along 120^{o} planes. As a means of checking the accuracy of this simulation, a static, three sabot configuration, Figure 7, was also fabricated.

The projectile was fabricated from stainless steel. It has a diameter of 50.8mm (2 inches), a length to diameter ratio of 10.5, and a 30^{o} total included angle conical nose. Fifty static pressure orifices are positioned on the surface between the 120^{o} planes of symmetry. With the exception of four orifices distributed about the conical forebody, no taps were located outside of these meridians. The splitter plates were fabricated from 6.35mm (0.25 inch) thick stainless steel plates having dimensions of 0.41m by 0.44m. The leading edges of the splitter plates are chamfered at a 15^{o} angle. No pressure taps are located on the splitter plates. The sabot is fabricated from brass. It has cylindrical inner and outer surfaces of radii 25.4mm and 76.2mm, respectively. The leading edge of the sabot has a 40^{o} chamfer. Fifty pressure orifices are located on the chamfer, inner cylindrical surface, and side planes of the sabot component. The projectile, splitter plate, and sabot geometry are presented in scaled dimensions in Figure 8.

---

9. *K. Orlik-Ruckermann, "Half and Full-Model Experiments on Slender Cones at Angle of Attack," AIAA JSR, Vol. 11, No. 9, September 1973.*

10. *K. Orlik-Ruckermann, "Supersonic Dynamic Stability Experiments on the Space Shuttle," AIAA JSR, Vol. 9, No. 9, September 1972.*

Tests were conducted in the Hypersonic Leg of the NASA Langley Unitary Plan Facility. The projectile was mounted on a sting extending from a window blank, while the sabot was mounted on the main traveling sting centered in the tunnel. This arrangement precluded the acquisition of schlieren or shadowgraph optics. Pressure tubing was 0.050" transitioning into 0.070" stainless steel having a length of 4.6m. Pressure tubing was taken out of the tunnel and into a Scanivalve transducer. The geometry of the 4 x 4 foot test section and model arrangement permitted the sabot component to move relative to the projectile over an angular range from 0^{o} to 15^{o} in pitch and laterally from 3.2mm to 114mm. To maintain symmetry, the sabot component was not rolled or yawed during testing.

Tests were conducted at a Mach number of 4.5 which is representative of actual projectile flight Mach numbers; however, flight Reynolds number was not replicated. A summary of test and flight conditions are:

	M_∞	Re/m	T_{s_∞} (^{o}K)	P_{s_∞} (N/m^2)
Wind Tunnel	4.5	6.6×10^6	353	2.45×10^5
Free Flight	4.5	8.9×10^7	1487	2.93×10^7

In the initial formulation of the test, this failure to duplicate free flight Reynolds number was not considered serious, i.e., main emphasis was on the inviscid flow structure. Unfortunately, the test results show regions of shock boundary layer interaction and separated flow having strong influences during the early phases of sabot discard.

A variety of different combinations of components were tested. These include: sabot alone; single sabot component and projectile (with and without splitter plates); and three sabot components. Some of the data were taken to examine the effects of asymmetry in the discard pattern upon the flow properties; however, for the present discussion, only the symmetric data will be addressed.

IV. TEST RESULTS

A. Sabot Alone

The instrumented sabot component was tested singly in order to obtain data on the free flight aerodynamics of the shape. Surface pressure data along the plane of symmetry of the sabot component are given for angles of attack of 0^{o}, 8^{o}, and 16^{o} in Figure 9. As would be expected, the pressure on the front chamfer surface is high; however, it shows relatively small variation with angle of attack. The predictions of simple Newtonian theory are considerably below the measured values and show a much wider change with pitch. On the underside of

the sabot, the pressures are significantly lower reflecting the effects of expansion around the corner. The Newtonian predictions are better in this region.

Also shown on the figure is the pressure variation predicted by a semi-empirical shock expansion theory suggested by Siegelman[11]. This model assumes the flow has a stagnation point at the leading edge of the sabot (NB: for a freestream Mach number of 4.5 and a turning angle of 40^{o}, a two dimensional wedge flow would be at the extreme limit of attached shock solution), has a sonic point at the corner, and this is followed by a Prandtl-Meyer expansion through an angle of 40^{o}. The pressure distribution on the front chamfer is linearly interpolated between the stagnation pressure behind a normal shock and the associated sonic pressure. The pressure on the underside is simply assumed constant. While this model produces a good picture of the flow within the range of angle of attack, it is not sensitive to change in this angle.

B. Symmetry Analysis

In order to examine the effectiveness of the splitter plates in generating a flow similar to that with three sabot components, tests were conducted with three components arranged in a fixed geometry. These results are compared with the results with splitter plates installed.

The test arrangement is shown in Figure 7. Two additional sabot components are attached to the sting supporting the projectile. The third, instrumented sabot is supported on the main traversing sting. The sabot components are positioned at 0^{o} pitch relative to the projectile and at a lateral separation of 0.75 d (1.5 inches). This separation was selected since preliminary analysis indicated that the area between the bodies would be sufficient to pass all of the mass flow captured by the entrance area defined by the outer edge of the sabot components. This is analogous to the starting of (or normal shock swallowing problem) a supersonic inlet. For the splitter plate tests, the positioning of the single sabot component was identical to that described above.

The pressure distributions measured on the projectile and sabot component are compared in Figure 10. The two sets of data agree qualitatively quite well. The pressure on the front chamfer of the sabot is nearly identical in both cases. The peak pressure on the projectile surface is due to the impingement of the shock wave off the sabot. In both cases its location is identical; however, with three sabots present, the peak is higher than that measured with the

---

11. *D. Siegelman and P. Crimi, "Projectile/Sabot Discard Aero-Dynamics," Ballistic Research Laboratory, CR-00410, December 1979.* (AD#A080538).

splitter plates. Related to this, the pressure level ahead of the peak is lower with the three sabot results. These variations are due to the increased viscous effects associated with the splitter plates. The plates have boundary layers on their surfaces and develop a corner flow at intersection with the body. These type flows have been demonstrated to interact with entrance shocks on the sidewalls of 2-D supersonic inlets[12]. In the present case, the viscous effects associated with the splitter plates thicken the boundary layer on the body and extend the shock boundary layer interaction region downstream from the intersection point while reducing the height of the peak. In view of the pressure levels, it seems likely that the boundary layer has separated; however, correlated oil flow and heat transfer data would be needed to confirm this fact.

The rapid rise in pressure on the projectile surface is associated with the impingement of the sabot shock wave. The equally rapid decay of this pressure peak is due to the arrival of the corner expansion from the sabot. The decay of pressure on the projectile surface is similar in both test cases.

On both the underside and lateral side of the sabot component, a secondary compression is around S/d = 5, Figure 10. The peak values are nearly identical in both cases; however, the location is further downstream in the case of the three sabot arrangement. Pressure contours have been constructed from the measurements in these tests and tend to emphasize the strong qualitative agreement between the two flows, Figure 11.

Based upon a comparison between the test data in the case with three sabot components installed and with a single sabot component and splitter plates, it is felt that while exact quantitative agreement is not arrived at due to greater viscous interactions observed with the splitter plates installed, sufficiently good qualitative comparison is developed to conclude that the test technique is valid within the approximations and limitations of any scale model wind tunnel experiment.

C. Wave Form Analysis

The three sabot configuration provides an opportunity to investigate the origin of some of the pressure pulses measured on the projectile and sabot surfaces. Since one of the sabot segments can be moved while the others remain fixed, it is possible to infer the shock structure from changes in the surface pressure distributions measured as the sabot segment is moved.

---

12. *G. Paynter, "Analysis of Weak Glancing Shock/Boundary Layer Interactions," AIAA Paper No. 79-0144, January 1979.*

With the two fixed sabot segments set at 0^{o} pitch and a separation of 0.75 d, the movable component was traversed axially over a range of 1.5 d in the forward direction. The resulting surface pressure distributions on the projectile and sabot component (which is being moved) are shown in Figures 12a and 12b. As the sabot component is moved forward at 0.5 d increments, the peak pressure on the projectile surface moves forward at similar increments. This indicates that the peak is associated to the shock wave from the moving sabot component. However, examination of the pressure distribution on the moving sabot component shows that as this component moves axially forward, the peak on the underside and lateral side move rearward a similar amount relative to the sabot. This indicates that peaks are, in part, associated with adjacent, fixed sabot components. It is interesting to note that the pressure on the underside increases as the sabot component moves forward while that on the lateral side decreases. This may be due to a tendency to develop a shock coalescence on the underside between the reflected shock from the body and the transmitted shocks from adjacent sabot components.

A qualitative (i.e., handwaving) schematic of the shock propagation from the sabot to the body and back is presented in Figure 13. In this illustration, the view is along planes perpendicular to the axis of the projectile at various axial stations. For convenience, planes of symmetry are used. In Figure 13a, the shock wave is seen propagating away from the sabot component. Undoubtedly, the shock strength off the front chamfer surface is the greatest. Due to the geometry of the arrangement, the distance from the sabot to the planes of symmetry is less than that to the projectile surface; therefore, reflection occurs initially on these surfaces and moves toward the axis, Figure 13b. Likewise, the shock moves back toward the body and reflects initially from the lateral sides of the sabot, Figures 13c and 13d. At this point, the waves reflected from the symmetry planes represent transmitted shocks from adjacent sabot components, while the reflection off the projectile is associated with the particular sabot in question. The waves move around the lateral surfaces and across the underside of the sabot merging with the reflected wave from the projectile surface, Figures 13e and 13f. The sequencing of the waves can be observed in the pressure traces presented in Figures 10 and 12.

D. Sabot Discard Sequence.

From the measurements taken within the test matrix, a set of data is selected which represents the range of sabot geometries in an actual discard sequence, Figure 14.

At the closest gap distance, $\Delta Y = 0.064$ d, and zero pitch angle, the pressure distribution shows signs of a stagnation region within the sabot front chamfer followed by a nearly one-dimensional expansion of the flow through a sonic point at the sabot corner. At the free flight Mach number, the following flow properties may be computed:

$$M_\infty = 4.5: \quad P_{t_2}/p_\infty = 26.51$$

$$p_2^*/p_\infty = 14.01$$

On a 15^o half angle cone:

$$p_c/p_\infty = 3.23$$

On a 40^o wedge:

$$p_w/p_\infty = 19.63$$

Comparison of some of these values with the pressure levels measured on the sabot and projectile, Figure 14a, indicates that even on the surface of the cone, S/d = 9, the flow is altered by the shock-boundary layer interactions and flow separation. A spark shadowgraph of the flow over the forward portion of a sabot/projectile during early discard (M_∞ = 1.4) illustrates this behavior, Figure 15. The excursions in pressure on the front chamfer of the sabot may be one of a variety of shock on shock interactions between the projectile and sabot shocks[13].

As the sabot moves away from the body, the nature of the flow changes, Figure 14b. The leading edge of the sabot is now in relatively undisturbed flow. The pressure variation across this front chamfer surface is similar to that measured with the sabot mounted independently, Figure 9. The conical forebody of the projectile still exhibits pressure in excess of the conical flow prediction (the relaxation to this value does not occur until the furthest separation of this sequence). The cylindrical surface of the projectile shows the impingement of the sabot shock and subsequent peaks associated with successive shock reflections. The underside of the sabot is behaving in a manner similar to the flow model described by Siegelman[11]. There is apparently a sonic point at the shoulder followed by a Prandtl-Meyer expansion and arrival of the reflected and transmitted shocks from the projectile and adjacent sabots.

As the sabot continues to pitch away from the projectile, the impingement point of its shock moves aft along the projectile and the peak pressure begins to decay, Figure 14c and 14d. A strong recompression begins to develop in the flow. This may be due to a normal shock standing in the converging flow[11] similar to the terminal shock in a supersonic inlet. Alternatively, this could represent a quasi-isentropic compression of a converging supersonic flow established by

---

13. *B. Edney, "Effects of Shock Impingement on the Heat Transfer Around Blunt Bodies," AIAA J., Vol. 6, No. 1, January 1968.*

the channeling of the sabot components. In any case, it represents an interesting departure in the nature of the flow. The peak pressure on the sabot is moving aft as the sabot pitches away from the projectile. With the sabot designs typified in Figure 1 and Figure 3, the resulting lateral lift due to these elevated pressures is not optimal due to the reduction in surface area along the rear ramp.

In an attempt to utilize the interference loading to assist discard, a sabot was fabricated with thin aerodynamic surfaces (wings) on the rear of the ramp. The rounds were fired in a ballistic range and discard measured using sequential X-rays. The resulting angle of separation between the projectile and sabot component trajectories was increased from 2.1° to 3.8°. This increase in the rate of separation produces a 55% decrease in the length of the trajectory over which aerodynamic interaction can occur between the sabot components and the projectile.

V. SUMMARY AND CONCLUSIONS

A series of wind tunnel tests have been conducted at NASA Langley Unitary Plan Facility to examine the aerodynamics associated with sabot discard at hypersonic Mach numbers. The data was limited to surface pressure measurements. To simulate the symmetric separation of three, non-rolling sabot components, a splitter plate technique was used which produced excellent qualitative agreement with the multiple component baseline. Quantitatively, the effects of increased viscous interactions due to the splitter plates altered the exact pressure levels.

Tests indicated that simple Newtonian theory is not adequate to treat the flow field, even that on a single sabot component in independent free flight. The effects of shock-boundary layer interaction are quite important. The experimental results suggested a design modification which was successfully demonstrated in hardware tests.

In order to define better the flow field, additional testing is required with improved instrumentation on the projectile and sabot. Surface flow visualization would better define the nature of shock-boundary layer interaction. Selected probing of the boundary layers and flow field could add important definition to the flow structure. Additionally, complimentary ballistic firings to measure the shock patterns between the bodies would be worthwhile.

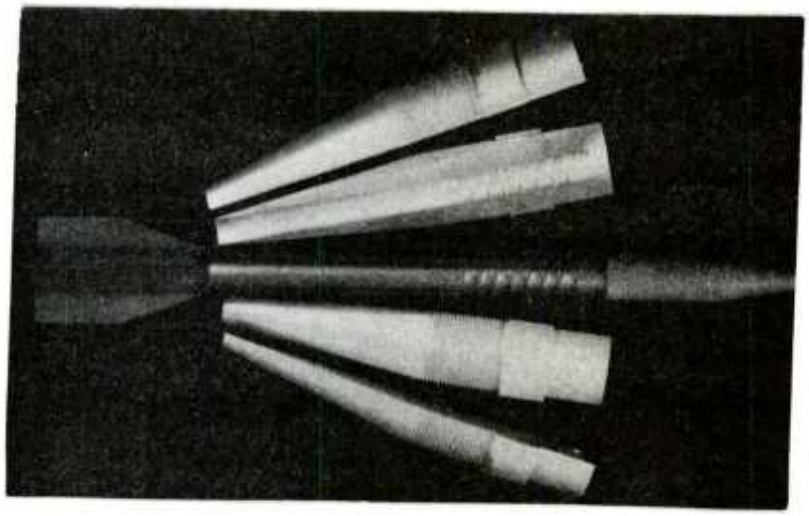

Figure 1. Typical Saboted Projectile: 60mm Round

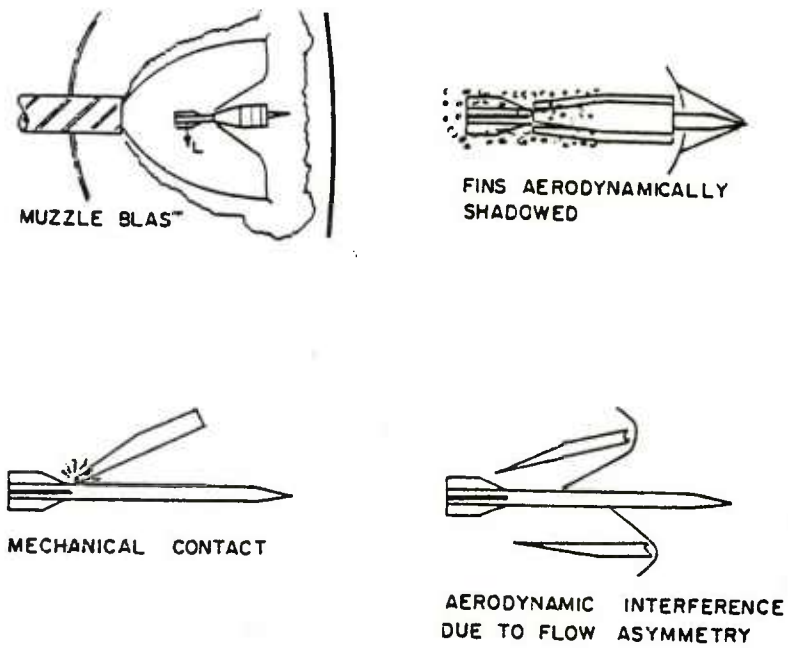

Figure 2. Schematic of Post-Launch Disturbances

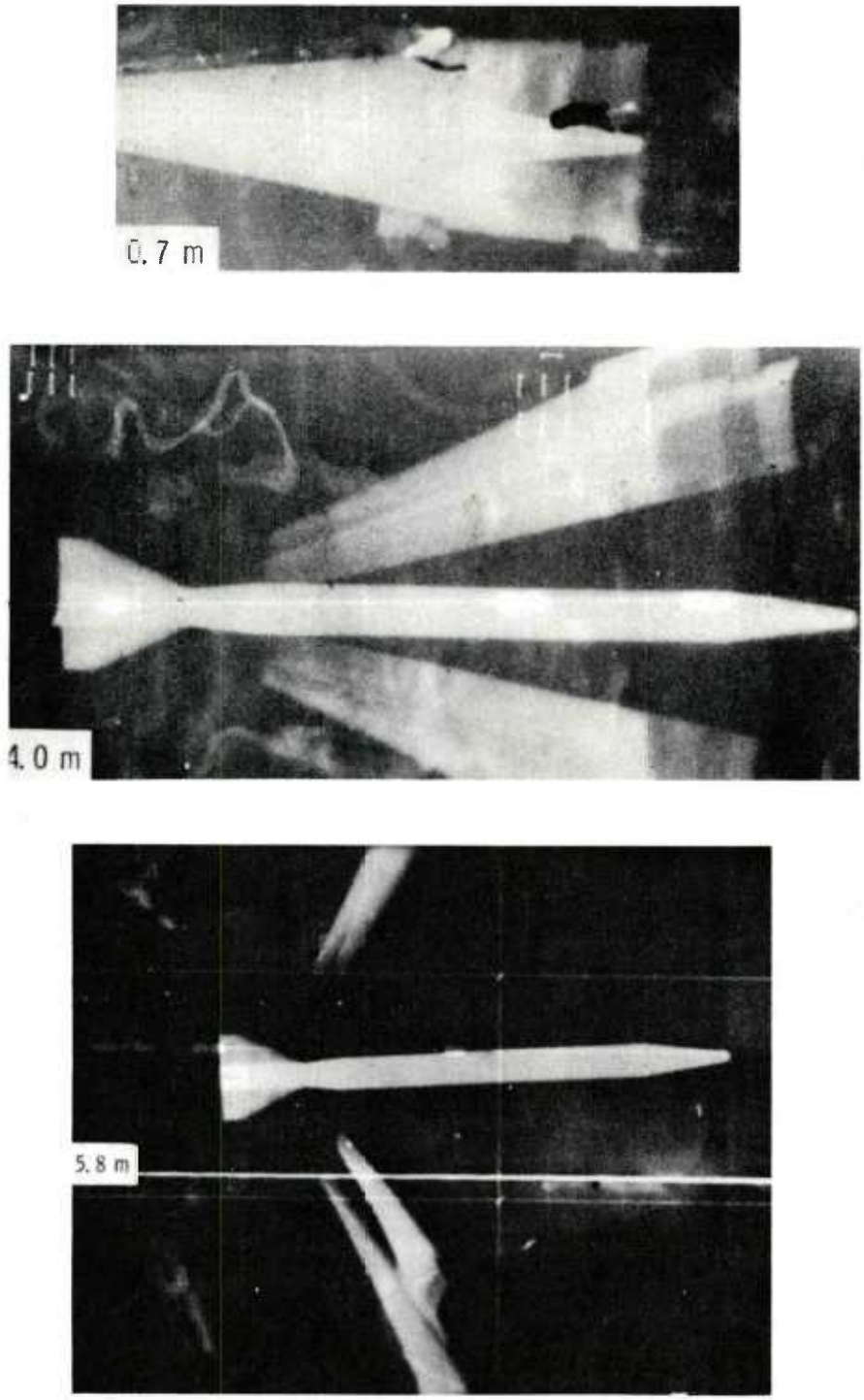

Figure 3. Sample X-ray Sequence of the Sabot Discard from 75mm Round Launched from Smoothbore Gun

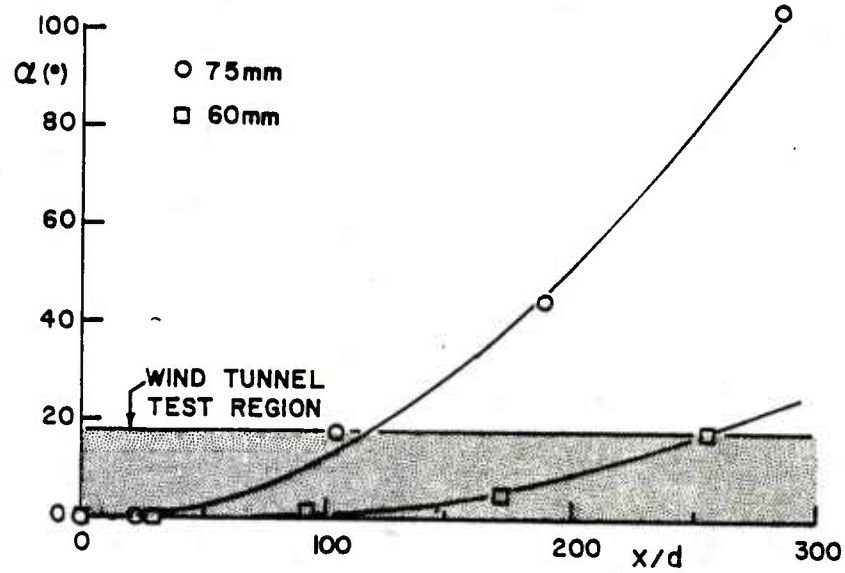

Figure 4a. Measured Variation in Sabot Angle of Attack During Discard

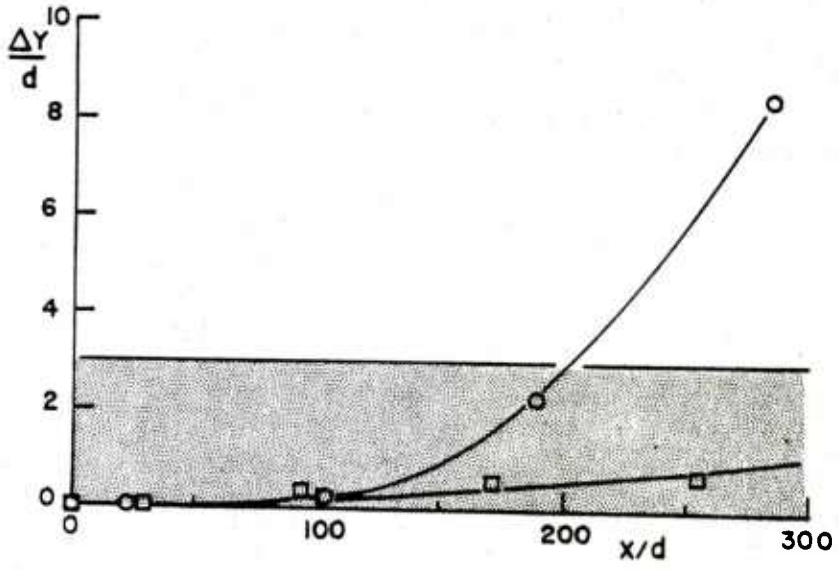

Figure 4b. Measured Variation in Sabot Lateral Separation during Discard

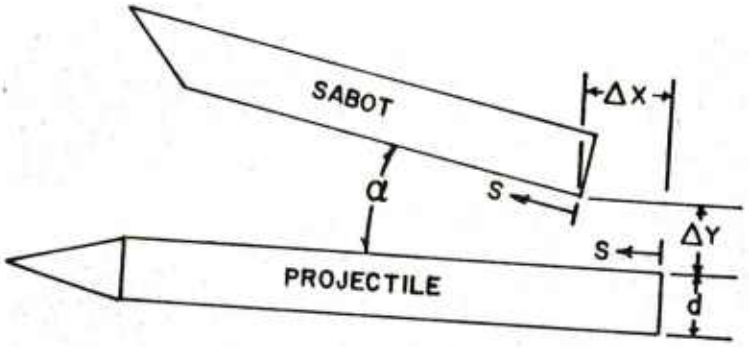

Figure 5. Separation Coordinates

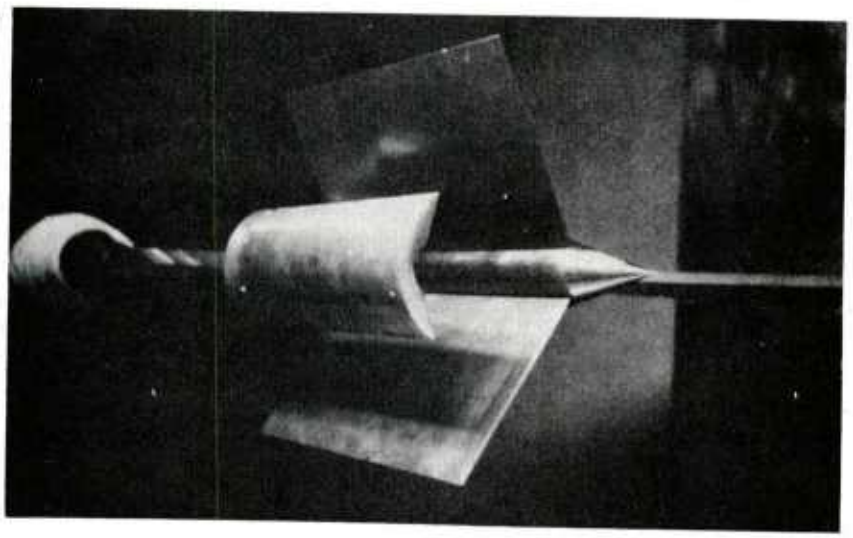

Figure 6. Photograph of Sabot and Projectile with Splitter Plates Installed

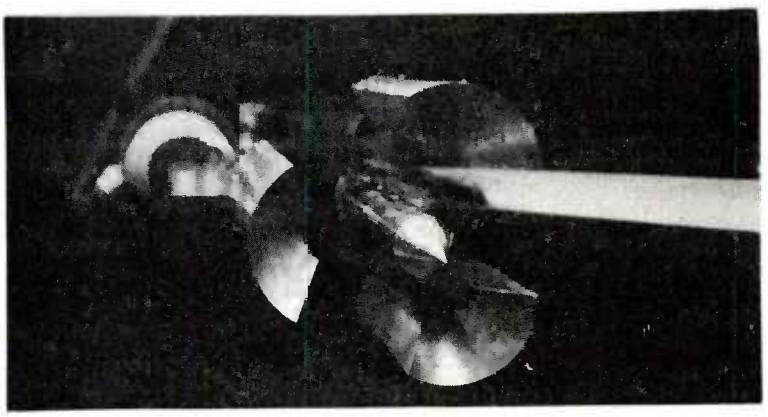

Figure 7. Photograph of Three Sabot Components and Projectile

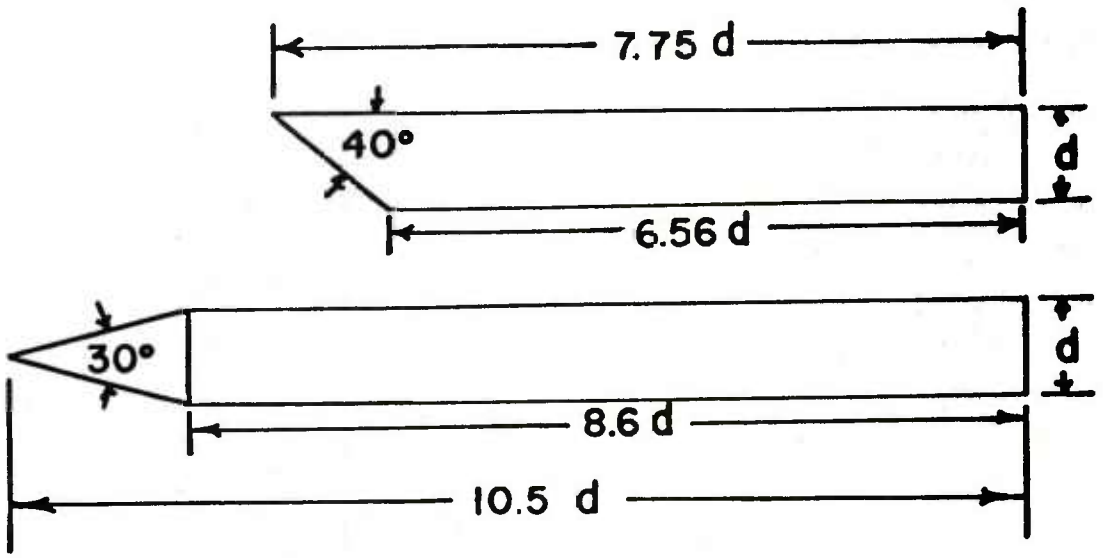

Figure 8a. Scaled Dimensions (d = 0.0508m, 2")

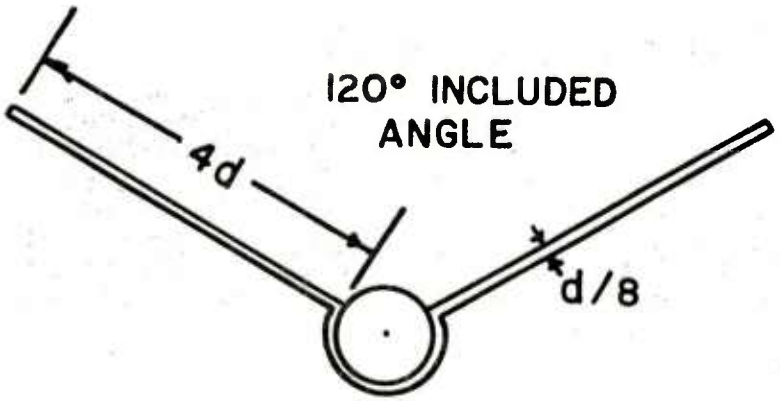

Figure 8b. Scaled Dimensions (d = 0.0508m, 2")

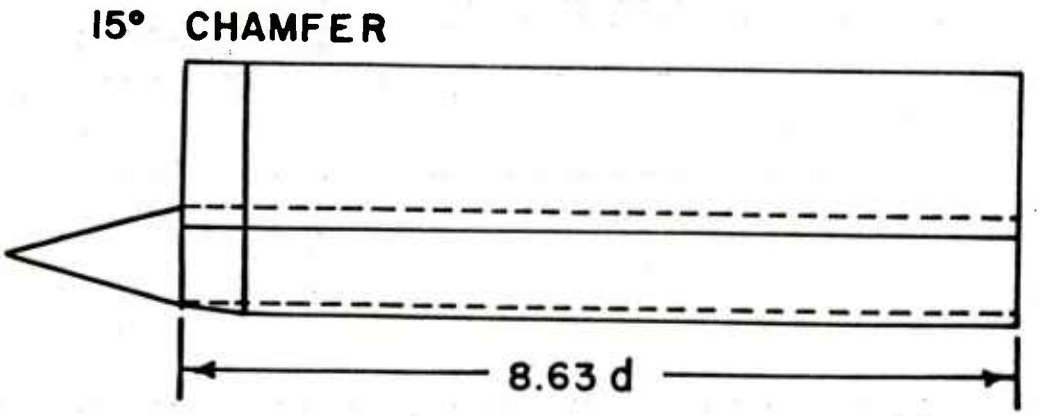

Figure 8c. Scaled Dimensions (d = 0.0508m, 2")

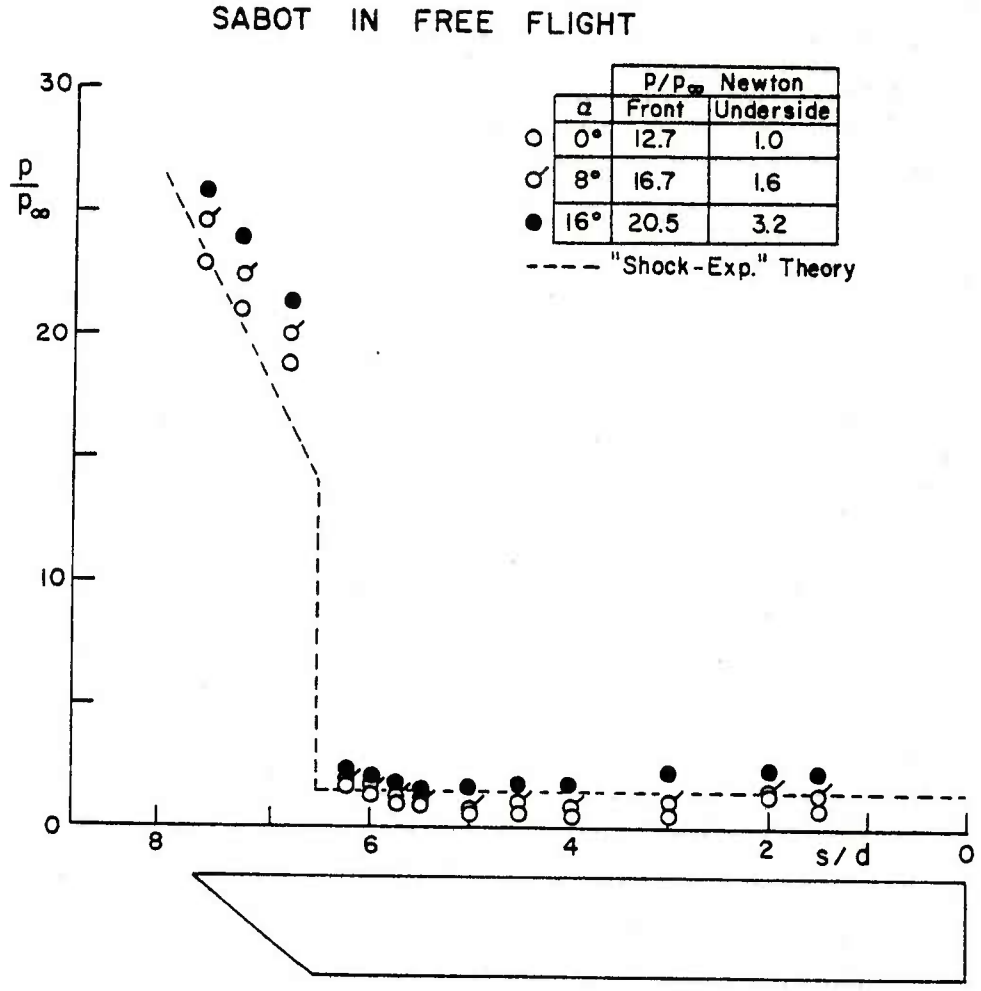

Figure 9. Variation in Pressure Distribution Along Centerline of Sabot with Sabot Mounted Independently in Wind Tunnel

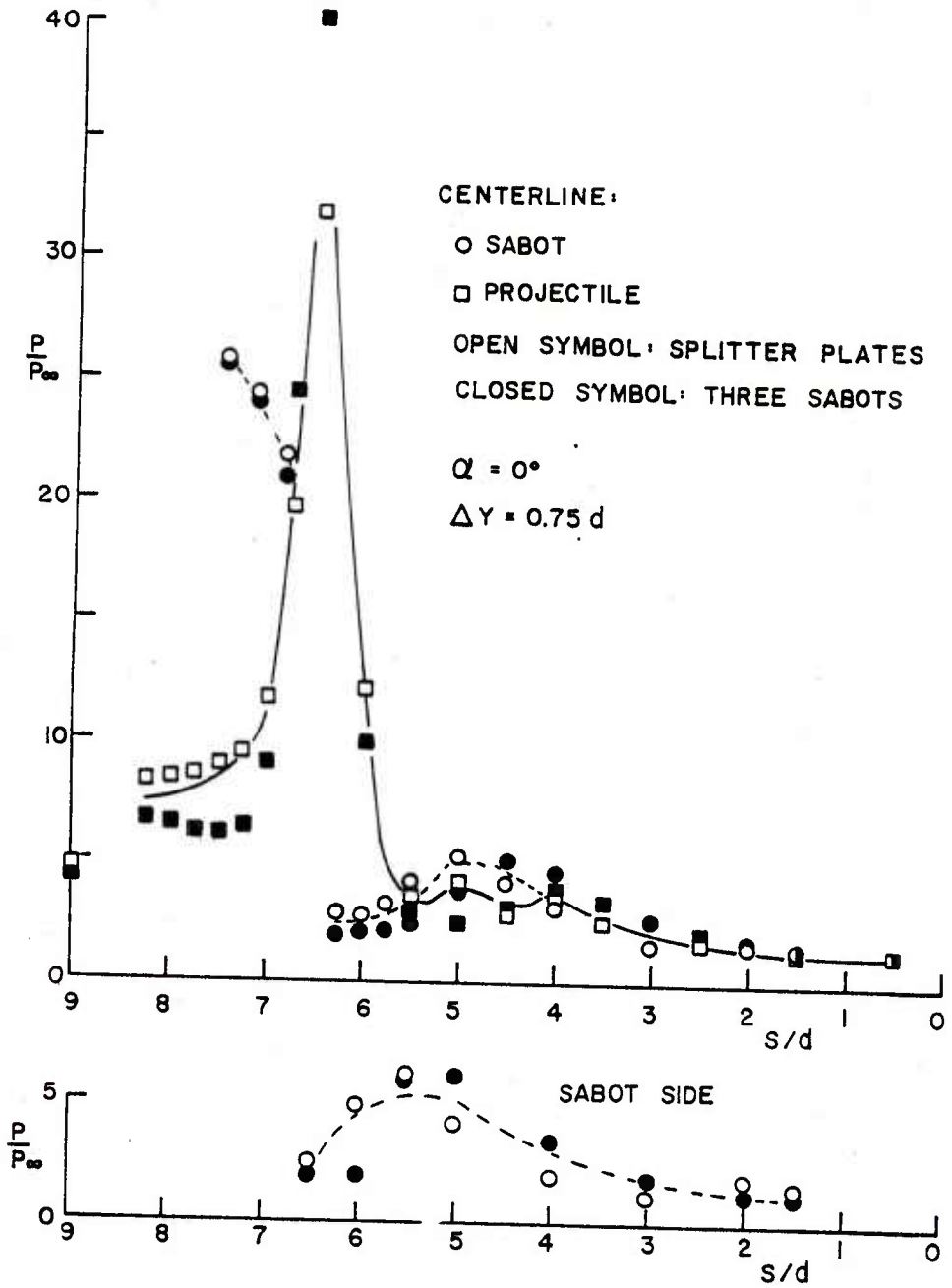

Figure 10. Pressure Distributions Along Centerlines of Sabot and Projectile for Symmetry Check Cases, $\alpha = 0^{0}$, $\Delta X = 0$, $\Delta Y = 0.75$ d

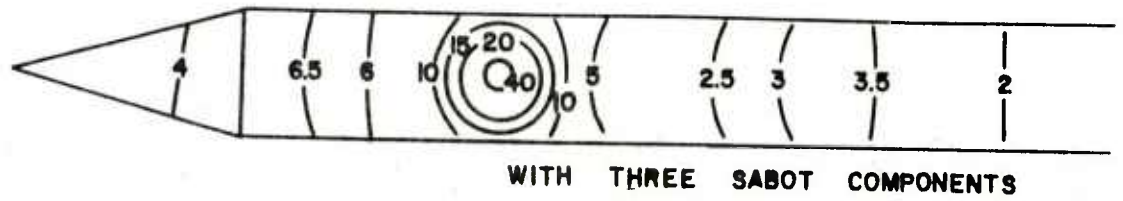

WITH THREE SABOT COMPONENTS

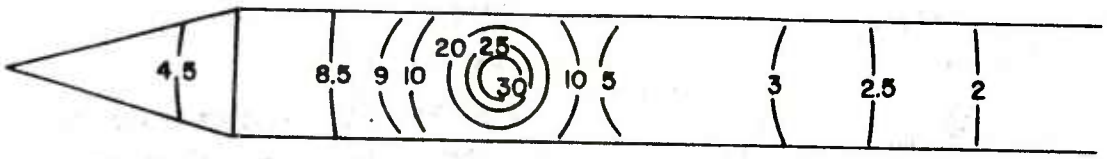

WITH ONE SABOT COMPONENT
AND SPLITTER PLATES

Figure 11a. Pressure Contours on Projectile Surface for Symmetry Check Case

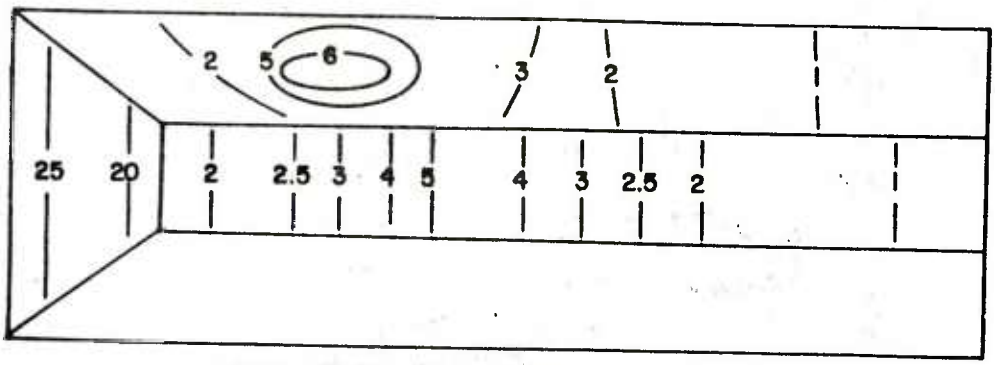

WITH THREE COMPONENTS

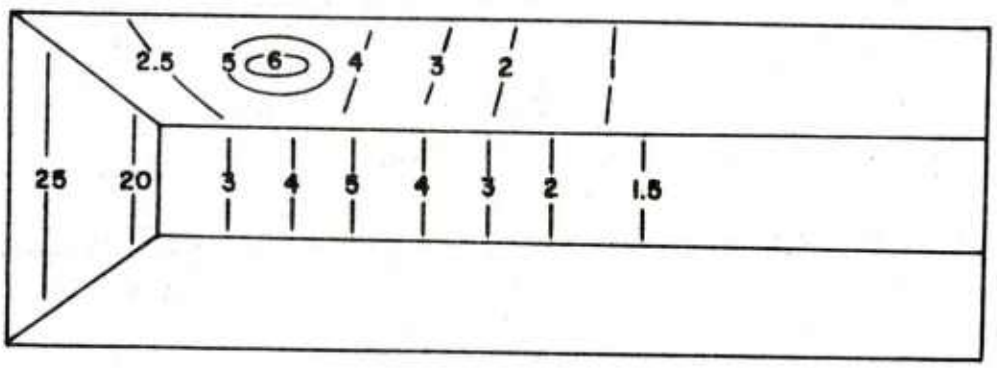

WITH SPLITTER PLATES

Figure 11b. Pressure Contours on Sabot Surface for Symmetry Check Case

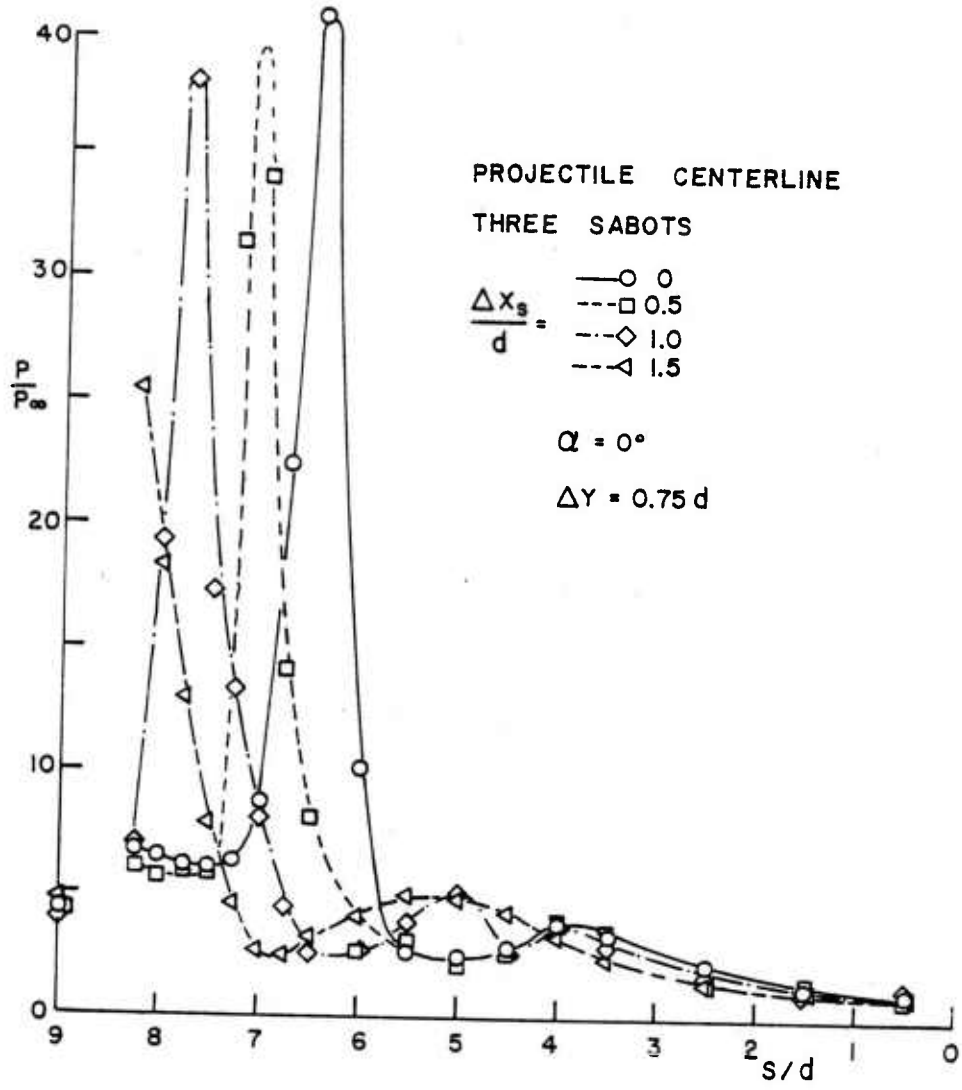

Figure 12a. Projectile Centerline Pressure Distribution with Three Sabots Installed, One of Which is Being Traversed Forward

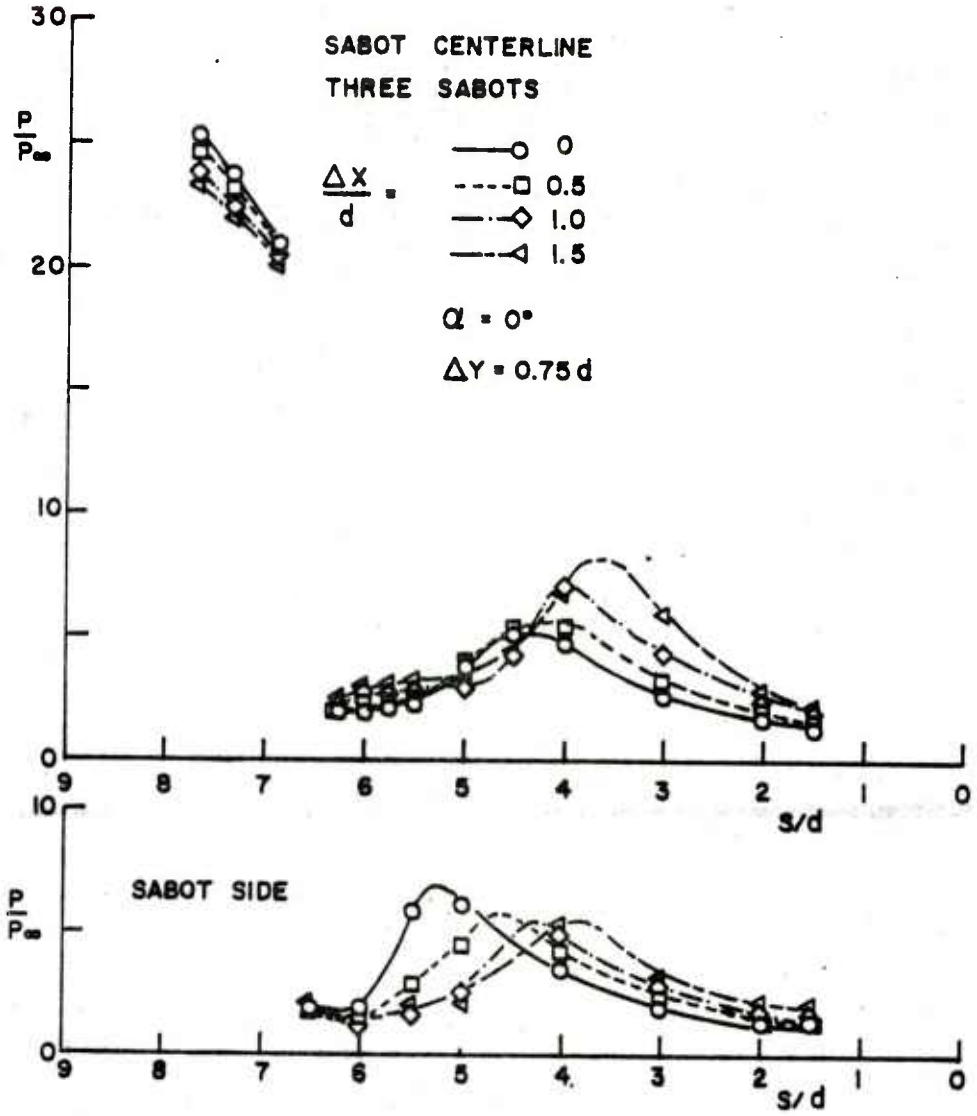

Figure 12b. Sabot Pressure Distribution on Moving Sabot with Three Sabots Installed

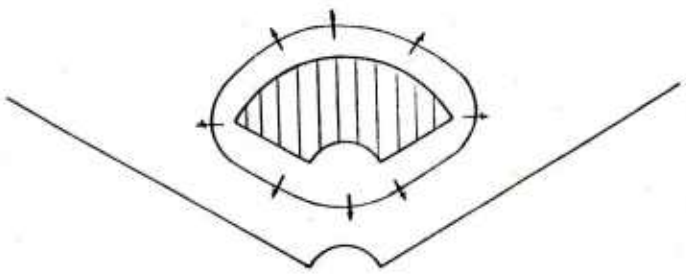

a.

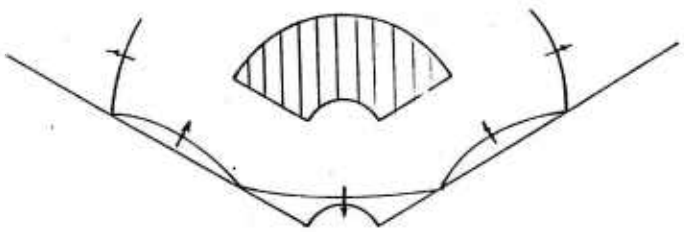

b.

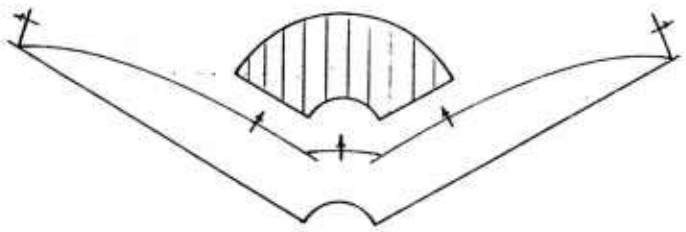

c.

Figure 13. Schematic of Shock Propagation Between Sabot and Projectile Viewed in Planes Perpendicular to the Projectile Axis of Symmetry at Sequential Axial Stations

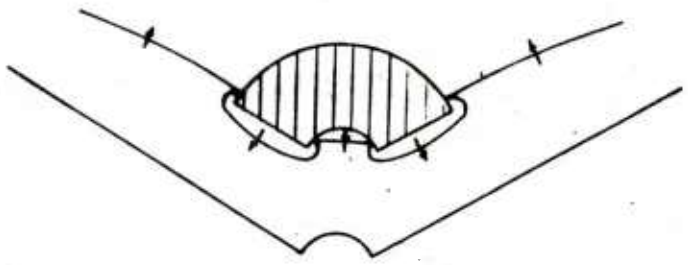

d.

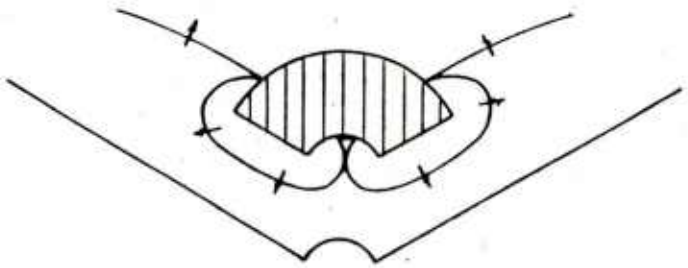

e.

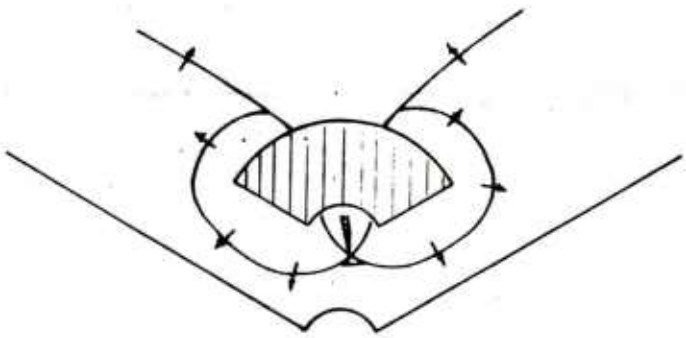

f.

Figure 13. Schematic of Shock Propagation Between Sabot and Projectile Viewed in Planes Perpendicular to the Projectile Axis of Symmetry at Sequential Axial Stations

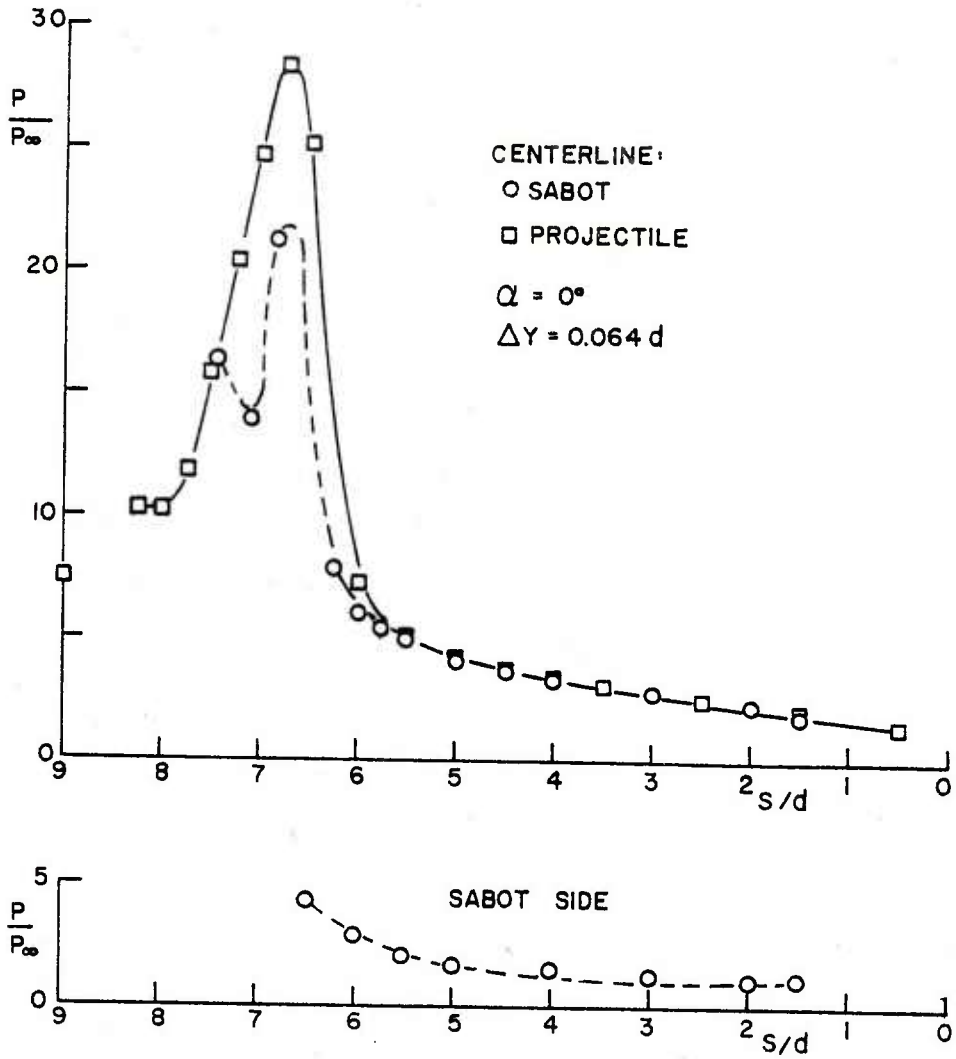

Figure 14a. Pressure Distributions During Simulated Sabot Discard, $\alpha = 0^{0}$, $\Delta X = 0$, $\Delta Y = 0.064$ d

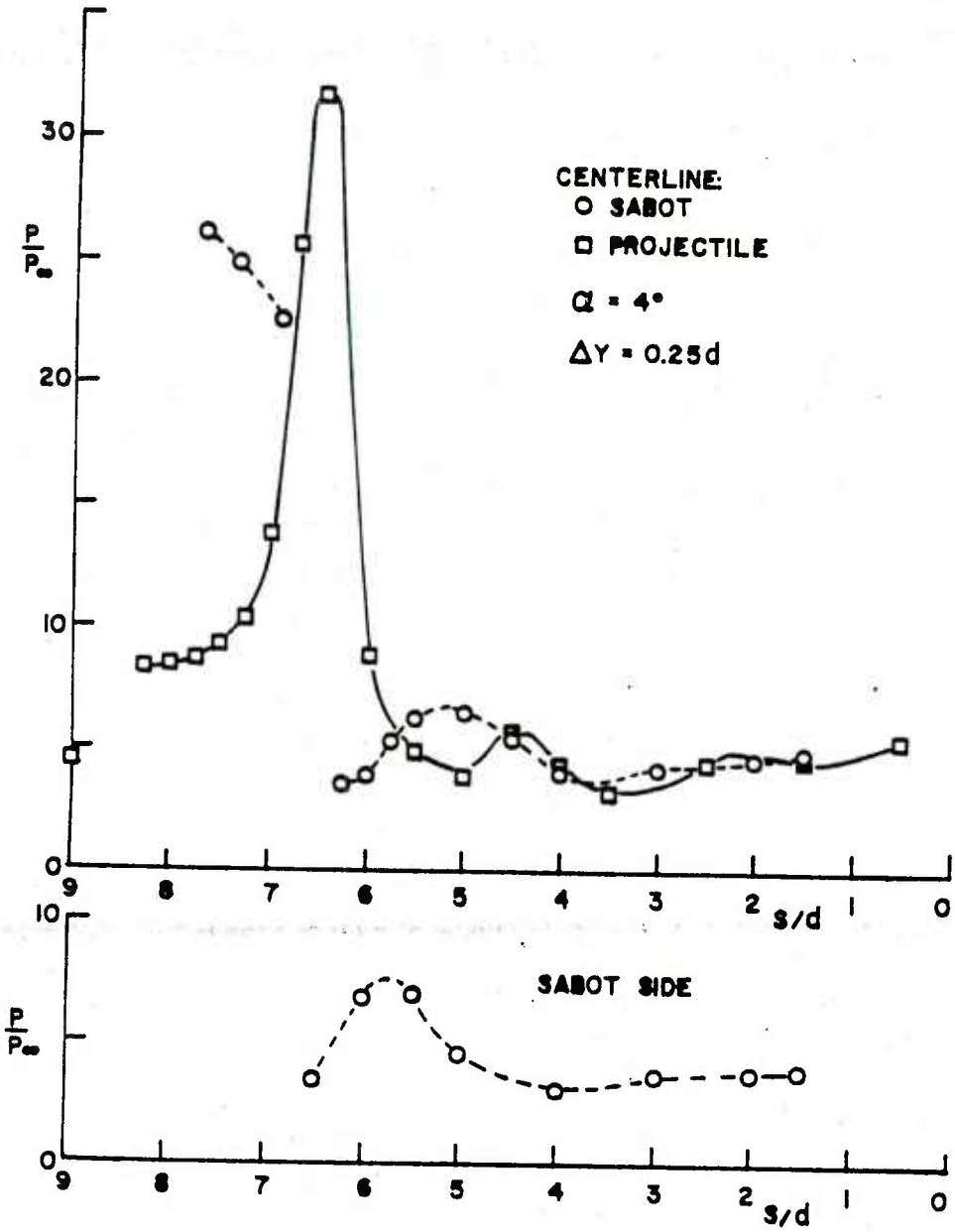

Figure 14b. Pressure Distributions During Simulated Sabot Discard, $\alpha = 4^{\circ}$ $\Delta X = 0$, $\Delta Y = 0.25$ d

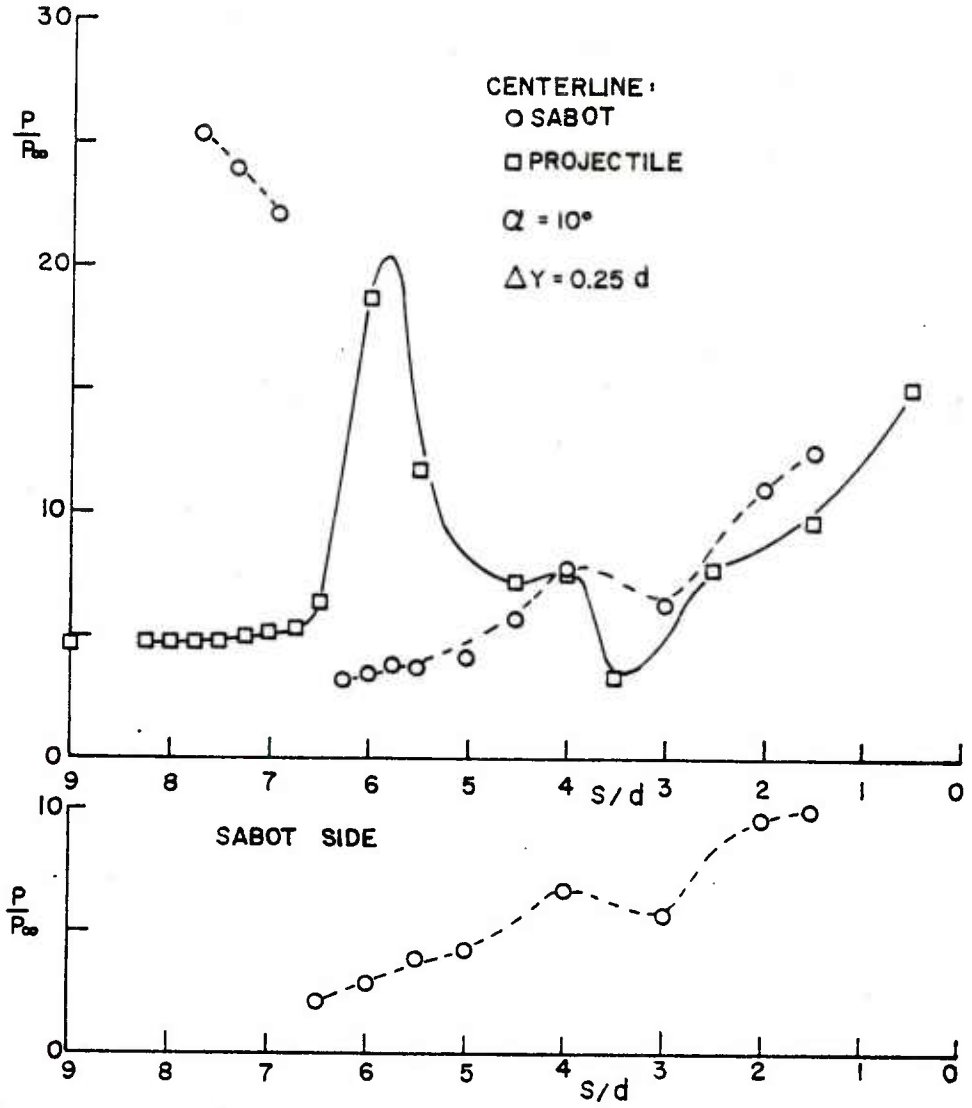

Figure 14c. Pressure Distributions During Simulated Sabot Discard, $\alpha = 10^0$, $\Delta X = 0$, $\Delta Y = 0.25$ d

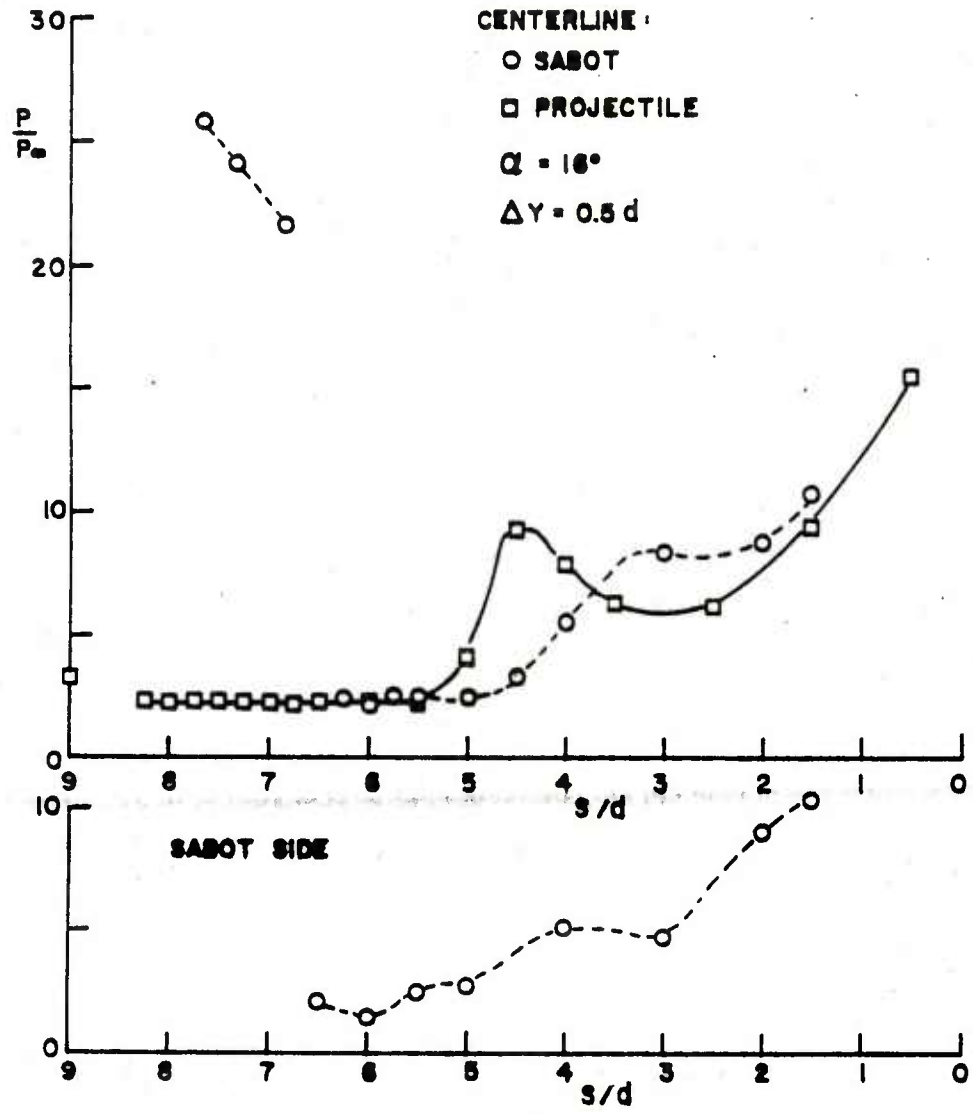

Figure 14d. Pressure Distributions During Simulated Sabot Discard, $\alpha = 18^{0}$, $\Delta X = 0$, $\Delta Y = 0.5$ d

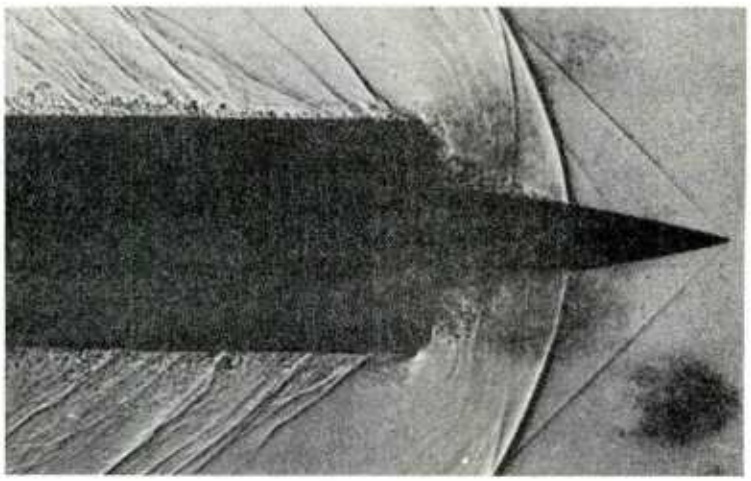

Figure 15. Spark Shadowgraph of Flow over Nose of Saboted Projectile, $M_\infty = 1.4$

ACKNOWLEDGMENT

The author wishes to thank the staff of the NASA Unitary Plan Facility for their assistance and suggestions during and preceding the experimental program. Charlie Jackson, Odell Morris, and Garland Wilson all contributed their considerable expertise. Thanks also to Tom Young of the Naval Surface Weapons Center, White Oak, who designed and fabricated the models tested.

REFERENCES

1. H. Conn, "The Influence of Sabot Separation on the Yawing Motion of a Cone," Defense Research Establishment at Valcartier, Canada, June 1970, TN 1849/70.

2. W. Glauz, "Estimation of Forces on a Flechette Resulting from a Shock Wave," Midwest Research Institute, Kansas City, MO, May 1971, R3450-E.

3. E. Schmidt and D. Shear, "Aerodynamic Interference During Sabot Discard," AIAA JSR, Vol. 15, No. 3, May-June 1978, pp 162-167.

4. Anon, "Proceedings of the Fourth Aircraft/Stores Compatibility Symposium," Joint Technical Coordinating Group for Munitions Development, Air Force Armaments Laboratory, Eglin, FL, 12-14 October 1977.

5. W. Sears, Ed., "Aerodynamic Interference," AGARD Conference Proceedings No. 71, September 1970.

6. W. Sayano, C. Erickson, and J. Murphy, "Aerodynamic Interference Associated with Two Parallel Bodies in Close Proximity in Hypersonic Flow," AFFDL, Wright-Patterson AFB, OH, TR AFFDL-64-158, December 1964.

7. K. Knight, "Improved Numerical Simulation of High Speed Inlets Using the Navier-Stokes Equations," AIAA Paper 80-0383, January 1980.

8. R. Buggeln, H. McDonald, J. Kreskovsky, and R. Levy, "Computation of Three-Dimensional Viscous Supersonic Flows in Inlets," AIAA Paper No. 80-0194, January 1980.

9. K. Orlik-Ruckermann, "Half and Full-Model Experiments on Slender Cones at Angle of Attack," AIAA JSR, Vol. 11, No. 9, September 1973.

10. K. Orlik-Ruckermann, "Supersonic Dynamic Stability Experiments on the Space Shuttle," AIAA JSR, Vol. 9, No. 9, September 1972.

11. D. Siegelman and P. Crimi, "Projectile/Sabot Discard Aero-Dynamics," Ballistic Research Laboratory, CR-00410, December 1979.

12. G. Paynter, "Analysis of Weak Glancing Shock/Boundary Layer Interactions," AIAA Paper No. 79-0144, January 1979.

13. B. Edney, "Effects of Shock Impingement on the Heat Transfer Around Blunt Bodies," AIAA J., Vol. 6, No. 1, January 1968.

DISTRIBUTION LIST

No. of Copies	Organization
12	Commander Defense Technical Info Center ATTN: DDC-DDA Cameron Station Alexandria, VA 22314
1	Director Defense Nuclear Agency Washington, DC 20305
1	HQDA (DAMA-WSA, MAJ Csoka) Washington, DC 20310
1	HQDA (DAMA-CSM, LTC Germann) Washington, DC 20310
1	Director US Army BMD Advanced Technology Center P.O. Box 1500, West Station Huntsville, AL 35804
1	Commander US Army Materiel Development & Readiness Command ATTN: DRCDMD-ST 5001 Eisenhower Avenue Alexandria, VA 22333
1	Commander US Army Materiel Development & Readiness Command ATTN: DRCDL 5001 Eisenhower Avenue Alexandria, VA 22333
7	Commander US Army Armament Research & Development Command ATTN: DRDAR-TSS (2 cys) DRDAR-TDS, Mr.Lindner DRDAR-TDA, Mr. Blick DRDAR-LC-F, Mr.A.Loeb Mr. E. Friedman DRDAR-SEM, W.Bielauskas Dover, NJ 07801
7	Commander US Army Armament Research & Development Command ATTN: DRDAR-LCV, Mr. Reisman DRDAR-SCN, Mr. Kahn DRDAR-LC, Dr. Frasier DRDAR-SCW, Mr. Townsend DRDAR-SG, Dr. T. Hung DRDAR-LCT, E. Barrieres PM, XM788/789, LTC Delany Dover, NJ 07801
2	Commander US Army Armament Materiel Readiness Command ATTN: DRSAR-LEP-L, Tech Lib Rock Island, IL 61299
6	Director US Army ARRADCOM Benet Weapons Laboratory ATTN: DRDAR-LCB-TL Mr. W. Dock Dr. G. Carofano Mr. P. Alto DRDAR-LCB, Mr. T. Allen Mr. R. Billington Watervliet, NY 12189
3	Commander US Army Aviation Research & Development Command ATTN: DRSAV-E DRCPM-AAH Product Manager, AH-1 P.O. Box 209 St. Louis, MO 63166
1	Director US Army Air Mobility Research & Development Laboratory Ames Research Center Moffett Field, CA 94035

DISTRIBUTION LIST

No. of Copies	Organization
1	Commander US Army Communications Research & Development Command ATTN: DRDCO-PPA-SA Fort Monmouth, NJ 07703
1	Commander US Army Electronics Research & Development Command Technical Support Activity ATTN: DELSD-L Fort Monmouth, NJ 07703
3	Commander US Army Missile Command ATTN: DRDMI-R DRDMI-RBL DRDMI-RDK Redstone Arsenal, AL 35809
2	Commander US Army Missile Command ATTN: DRSMI-TLH (Ricks) DRSMI-YDL Redstone Arsenal, AL 35809
1	Commander US Army Natick Research & Development Command ATTN: DRXRE, Dr. D. Sieling Natick, MA 01762
1	Commander US Army Tank Automotive Research & Development Cmd ATTN: DRDTA-UL Warren, MI 48090
1	Commander US Army Jefferson Proving Ground ATTN: STEJP-TD-D Madison, IN 47250
1	Commander US Army Materials and Mechanics Research Center ATTN: DRXMR-ATL Watertown, MA 02172
1	Commander US Army Research Office ATTN: CRD-AA-EH P.O. Box 12211 Research Triangle Park NC 27709
2	Director US Army TRADOC Systems Analysis Activity ATTN: ATAA-SL, Tech Lib ATAA-S White Sands Missile Range, NM 88002
1	ODCSI, USAREUR & 7A ATTN: AEAGB-PDN (S&E) APO, NY 09403
3	Commander Naval Air Systems Command ATTN: AIR-604 Washington, DC 20360
3	Commander Naval Ordnance Systems Command ATTN: ORD-9132 Washington, DC 20360
2	Commander David W. Taylor Naval Ship Research & Development Center Aerodynamic Lab ATTN: Lib Div, Code 522 Bethesda, MD 20084

DISTRIBUTION LIST

No. of Copies	Organization
3	Commander Naval Surface Weapons Center ATTN: Code 6X, Mr. F.H. Maille Dr. J. Yagla Dr. G. Moore Dahlgren, VA 22448
1	Commander Naval Surface Weapons Center ATTN: Code 730, Tech Lib Silver Spring, MD 20910
1	Commander Naval Weapons Center ATTN: Code 553, Tech Lib China Lake, CA 93555
1	Commander Naval Research Laboratory ATTN: Tech Info Div Washington, DC 20375
1	Commander Naval Ordnance Station ATTN: Code FS13A, P. Sewell Indian Head, MD 20640
1	AFRPL/LKCC, C.D. Penn Edwards AFB, CA 93523
2	AFATL(DLDL, Dr. D.C. Daniel; Tech Lib) Eglin AFB, FL 32542
1	Guns Test Branch AD3246 TESTW/TETFG Eglin AFB, FL 32542
1	AFWL/SUL Kirtland AFB, NM 87117
1	ASD/XRA Wright-Patterson AFB, OH 45433

No. of Copies	Organization
1	Sandia Laboratories ATTN: Aerodynamics Dept Org 5620, R. Maydew Albuquerque, NM 87115
1	Director Jet Propulsion Laboratory ATTN: Tech Lib 4800 Oak Grove Drive Pasadena, CA 91103
1	Director National Aeronautics and Space Administration George C. Marshall Space Flight Ctr ATTN: MS-I, Lib Huntsville, AL 38512
4	Director National Aeronautics and Space Administration Langley Research Center ATTN: MS 185, Tech Lib Unitary Plan Facility C. Jackson O. Morris W. Corlett Langley Station Hampton, VA 23365
1	Director NASA Scientific & Technical Information Facility ATTN: SAK/DL P.O. Box 8757 Baltimore/Washington International Airport, MD 21240
1	AAI Corporation ATTN: Dr. T. Stastny Cockeysville, MD 21030
1	Advanced Technology Labs ATTN: Mr. J. Ranlet Merrick & Steward Avenue Westbury, NY 11590

DISTRIBUTION LIST

No. of Copies	Organization
1	Aerospace Corporation ATTN: Dr. T. Taylor P.O. Box 92957 Los Angeles, CA 90009
1	ARO, Inc. ATTN: Tech Lib Arnold AFS, TN 37389
1	ARO, Inc. Von Karman Gasdynamics Facility ATTN: Dr. J. Adams Arnold AFS, TN 37389
1	ARTEC Associates, Inc. ATTN: Dr. S. Gill 26046 Eden Landing Road Hayward, CA 94545
2	AVCO Systems Division ATTN: Dr. W. Reinecke Dr. D. Siegelman 201 Lowell Street Wilmington, MA 01887
1	Battelle Columbus Laboratories ATTN: J.E. Backofen, Jr. 505 King Avenue Columbus, OH 43201
1	Technical Director Colt Firearms Corporation 150 Huyshope Avenue Hartford, CT 14061
1	Flow Simulations Inc. ATTN: Dr. J. Steger 735 Alice Avenue Mountain View, CA 94041
2	General Electric Corporation Armaments Division ATTN: Mr. R. Whyte Mr.J. MacNeil Lakeside Avenue Burlington, VT 05401
1	Honeywell, Inc. Government & Aerospace Products Div. ATTN: Mail Station MN 112190 G. Stilley 600 Second Street, North Hopkins, MN 55343
3	Hughes Aircraft Company ATTN: Mr. R. Forker Mr. T. Edwards Mr. R. Flood Bldg 2, MST22B Centinella and Teale Streets Culver City, CA 90230
1	Martin Marietta Aerospace ATTN: Mr. A.J. Culotta P.O. Box 5387 Orlando, FL 32805
1	Olin Corporation Winchester-Western Division 275 Winchester Avenue New Haven, CT 06504
1	Rockwell Int'l Science Center ATTN: Dr. Norman Malmuth P.O. Box 1085 One Thousand Oaks, CA 91360
1	S&D Dynamics, Inc. ATTN: Dr. M. Soifer 755 New York Avenue Huntington, NY 11743
1	California Institute of Tech Guggenheim Aeronautical Lab ATTN: Tech Lib Pasadena, CA 91104
1	Director Applied Physics Laboratory The Johns Hopkins University Johns Hopkins Road Laurel, MD 20810

DISTRIBUTION LIST

No. of Copies	Organization
1	Massachusetts Institute of Technology Dept of Aeronautics and Astronautics ATTN: Tech Lib 77 Massachusetts Avenue Cambridge, MA 02139
1	Ohio State University Dept of Aeronautics and Astronautical Engineering ATTN: Tech Lib Columbus, OH 43210
2	Polytechnic Institute of New York Graduate Center ATTN: Tech Lib Dr. G. Moretti Route 110 Farmingdale, NY 11735
1	Director Princeton University Forrestal Research Center Princeton, NJ 08540
1	Southwest Research Institute ATTN: Dr. Peter S. Westine 8500 Culebra Road San Antonio, TX 78228

Aberdeen Proving Ground

Dir, USAMSAA
ATTN: DRXSY-D
DRXSY-MP, H. Cohen

Cdr, USATECOM
ATTN: DRSTE-TO-F

Cdr, USA CSL/EA
ATTN: SAREA-DE-W, M. Miller
Bldg E3516

Dir, Wpns Sys Concepts Team
Bldg E3516, EA
ATTN: DRDAR-ACW

USER EVALUATION OF REPORT

Please take a few minutes to answer the questions below; tear out this sheet and return it to Director, US Army Ballistic Research Laboratory, ARRADCOM, ATTN: DRDAR-TSB, Aberdeen Proving Ground, Maryland 21005. Your comments will provide us with information for improving future reports.

1. BRL Report Number _____

2. Does this report satisfy a need? (Comment on purpose, related project, or other area of interest for which report will be used.)

_____

_____

_____

3. How, specifically, is the report being used? (Information source, design data or procedure, management procedure, source of ideas, etc.) _____

_____

_____

4. Has the information in this report led to any quantitative savings as far as man-hours/contract dollars saved, operating costs avoided, efficiencies achieved, etc.? If so, please elaborate.

_____

_____

5. General Comments (Indicate what you think should be changed to make this report and future reports of this type more responsive to your needs, more usable, improve readability, etc.) _____

_____

_____

_____

6. If you would like to be contacted by the personnel who prepared this report to raise specific questions or discuss the topic, please fill in the following information.

Name: _____

Telephone Number: _____

Organization Address: _____

_____

_____